Liquid State Theory of Thermally Driven Segregation of Conformationally Asymmetric Diblock Copolymer Melts

Edwin F. David† and Kenneth S. Schweizer*

Departments of Chemistry and Materials Science & Engineering and Materials Research Laboratory, University of Illinois, 1304 West Green Street, Urbana, Illinois 61801

Received February 13, 1997; Revised Manuscript Received June 2, 1997⊗

ABSTRACT: Thermally induced packing correlations and apparent microphase spinodal boundaries are studied for conformationally asymmetric diblock copolymer melts using the "polymer reference interaction site model" (PRISM) theory. Microphase instabilities are deduced from predictions of the collective scattering intensities and are correlated with the degree of conformational mismatch. For diblocks interacting through attractive van der Waals forces, but where the Flory mean field χ-parameter is *identically zero*, the predictions reveal rich dependencies of the apparent microphase spinodal boundaries on the degree of structural asymmetry between blocks which are consistent with recent polyolefin diblock melt experiments. This demonstrates the importance of the coupling between local packing correlations and attractive interactions, and the fundamental inseparability of enthalpic and entropic contributions to the effective χ-parameter governing miscibility. Length-scale-dependent "effective compositions" above and near an apparent microphase spinodal temperature are also calculated. Large enrichments of the local composition are predicted in the highly fluctuating, low temperature, regime which depend on copolymer composition, density, and nonuniversal chain structural features. Marked enhancements of this clustering relative to melt behavior are predicted for concentrated diblock solutions. The present numerical calculations are also compared to previous analytical Gaussian thread model PRISM predictions, and general qualitative consistency is found. Numerical calculations for blends of the same polymers are also performed and demonstrate a very large reduction of concentration fluctuation effects and physical clustering for this macrophase separation case.

I. Introduction

In recent years experimental observations have demonstrated the sensitivity of macrophase and microphase boundaries on local polymer architecture[1−5] in model hydrocarbon alloys. The commercial significance and the fundamental scientific questions which these systems raise, as well as their potential for achieving novel materials properties, are among the reasons for continued interest in their structural and thermodynamic properties.[6,7] Leibler's original mean-field theory,[8] based in part on a formalism set forth by Helfand,[9] was the first to examine the microphase boundaries and ordered phase symmetries for diblock copolymer melts in the weak segregation regime. Since then, several refinements have been been put forth within highly coarse-grained, incompressible field theoretic approaches.[10] Most notable is the Brazovskii−Leibler−Fredrickson−Helfand (BLFH) fluctuation theory.[11,12] Other works within the same general approach account approximately for chain nonideality[13,14] and the temperature dependence of the peak scattering wave vector due to collective effects.[15] The significant limitations of these approaches due to "non-RPA" (random phase approximation) corrections have been recently worked out by Stepanow.[16] In addition, these incompressible field theoretic approaches have primarily employed conformational and interaction "symmetric" models for both conceptual and technical simplicity. Along somewhat different lines, others have adopted density functional,[17,18] lattice model,[19] and liquid state[20] approaches in order to study block copolymer equilibrium phenomena. To study the relationship between chemical and structural features of individual macromolecules and the bulk properties of the materials they compose, the microscopic compressible fluid theories[19,20] lend considerable insight beyond the issues which can be studied via heavily coarse-grained field theoretic approaches.

Most real copolymers possess some degree of asymmetry in monomer structure and interactions, and both coarse-grained and microscopic theories have begun to address such issues[19,21−32] in copolymers and blends. The conformational mismatches, along with the presence of attractive interactions, often lead to interesting monomer structure dependent phase behavior. For example, Bates et al.[1,5] have observed systematic variations in the absolute magnitude and molecular weight dependencies of the order−disorder transitions (ODT) temperatures with branching in a polyolefin diblock series. Given the ("bare") chemical similarity of the monomers in olefin copolymers, structural disparities are expected to be responsible for their often unexpected phase behavior. Analytical calculations of Schweizer[21] also suggest that while structural ("athermal") and chemical ("energetic") asymmetries originate from different physical features of the molecule, they cannot be treated as purely additive when it comes to questions involving the phase behavior of the liquid. This is in contrast to recent incompressible field theoretic approaches[25] wherein a spatially nonlocal excess entropic contribution to the effective χ-parameter governing phase behavior has been suggested to be responsible for the monomer-structure-dependent phase stabilities, with energetic effects being treated as a small additive empirical correction. Of course, in real systems all these effects are present at once, and those which may dominate are likely to be system specific to some degree. However, within the polyolefin class of molecules, which are generally highly *flexible* (i.e. their aspect ratios are roughly unity), we believe the coupled thermal and packing interactions are key to understanding the phase stabilities.[21,27,31,32] Furthermore, related theoretical[27,29] and simulation[33] studies on polymer blends suggest that

† Present address: Department of Chemistry, Brown University, Providence, RI 02912.

⊗ Abstract published in *Advance ACS Abstracts,* August 1, 1997.

S0024-9297(97)00202-7 CCC: $14.00

for flexible chains the noncombinatorial entropic contribution to demixing is small relative to the (correlated) energetic terms. Indirect evidence from polyolefin blend experiments[3] on the so-called isotope "swap effect" also indicate that nonadditive thermal and local packing interactions play a major, and probably dominant, role in polyolefin phase behavior.

In this study we investigate the role of coupled thermal and packing interactions in block copolymer melts, with an emphasis on the relation between local chain stiffness, intermolecular structure, and microphase separation. As discussed previously[20] within the PRISM theory of block copolymers, the local and long wavelength intermolecular structure of the conformationally and interaction *symmetric* model diblock liquid changes considerably as temperature is lowered. Strong like-monomer clustering takes place, leading via chain connectivity to a finite-size fluctuation stabilization of the disordered phase on the microdomain length scale and destruction of all critical and spinodal divergences. These enthalpy-induced packing modifications have also been observed in recent diblock copolymer simulations,[34,35] and appear to emerge from field theoretic approaches when the large non-RPA corrections are properly accounted for.[16] We expect similar effects in conformationally asymmetric block copolymers, although the precise magnitudes and trends will in general depend on the nonuniversal structural and energetic properties of the individual blocks. Furthermore, to explore the role of realistic dispersion interactions, we use *attractive* interactions between *all* species in the present work. This represents a departure from our previous model studies of symmetric systems,[20] where a repulsive AB−tail interaction was employed to mimic a net enthalpic driving force toward segregation. To stress the idea that energetics and structural correlations are nonseparable, and due to its relevance as a zeroth-order model for polyolefins, many predictions here are for the case in which the bare Flory χ_0 is *identically zero*. Within the simplest version of mean field theory these systems would be completely miscible. Thermally driven segregation thus occurs solely due to nonrandom mixing processes within this model.

The remainder of this paper is organized as follows. In section II the liquid state PRISM theory is briefly reviewed, and the chain and interaction potential models are presented. The small-angle scattering in diblock liquids is discussed in section III. Predictions for the apparent microphase spinodal boundaries are presented in section IV for chain models that mimic the intermolecular packing of real flexible diblock melts. A comparison to previous analytical PRISM predictions[21] is also made. Comparisons of the theoretical estimates for the microphase separation temperature and predictions for the small-angle scattering intensity of several conformationally asymmetric diblock melts with recent polyolefin experiments is presented in section V. Local structural correlations and length-scale-dependent effective compositions are studied in section VI. The influence of dilution of the melt by nonselective solvent is also briefly addressed. A comparison between the predictions for diblocks versus blends is presented in section VII. Section VIII contains a summary of this work.

II. Theory and Model

A. Theory and Closure Approximation. Polymer-RISM (PRISM) integral equation theory[36−38] describes the single chain structure through a set of averaged *intra*molecular pair distribution functions $\Omega_{MM'}(r)$. A tractable theory of block copolymers requires preaveraging over the interaction sites within each block (neglecting block-end effects). If $\omega_{M\alpha,M'\gamma}(r)$ represents the probability of finding site α of species M a distance r away from site γ of species M' on the same molecule, then

$$\Omega_{MM'}(r) \equiv \rho \sum_{\alpha\in M} \sum_{\gamma\in M'} \omega_{M\alpha,M'\gamma}(r) \tag{2.1}$$

where ρ is the molecular number density. *Inter*molecular correlations, $H_{MM'}(r)$, are related to Ω through a series of correlation pathways involving the so-called "direct correlation function", $C_{MM'}$, in an Ornstein−Zernike-like matrix equation

$$\hat{\mathbf{H}} = \hat{\Omega}\hat{\mathrm{C}}\hat{\Omega} + \hat{\Omega}\hat{\mathrm{C}}\hat{\mathrm{H}} \tag{2.2}$$

The (monomer-averaged) block−block *inter*molecular radial distribution functions, $g_{MM'}(r)$, can be calculated via the relation $H_{MM'}(r) = \rho_M\rho_{M'}[g_{MM'}(r) - 1]$, where $\rho_M = N_M\rho$ is the site number density of species M. The shorthand notation $\hat{f} \equiv \hat{f}(k)$ denotes Fourier transformed functions. The sites can represent either elementary functional groups such as a methylene unit, a monomer, or some collection of these which may constitute a coarse-grained "segment". The distinction between these levels of molecular structure description enters through the specification of the intrachain structure factor matrix, Ω, and the site-site intermolecular interactions, $v_{MM'}(r)$. If the single-chain structure is assumed to be unperturbed by the surrounding medium[39−41] (as in the Flory ideality hypothesis for dense melts utilized in the present work), then PRISM theory can be used to calculate the intermolecular pair correlations with use of a closure approximation involving the interactions. Detailed analytical and numerical applications to the structurally and interaction symmetric diblock copolymer are found in ref 20. Treatment of nonideal "chain-stretching" effects within liquid state theory has also been carried out,[41] but this results in only small corrections for the conditions of present interest.

Here we employ the "reference molecular Percus Yevick" (R-MPY) molecular closure[42,43] in its "high temperature approximation" (HTA) form

$$[\Omega^*\mathrm{C}^*\Omega]_{MM'}(r) = [\Omega^*(\mathbf{C}^{(0)} + \Delta\mathrm{C})^*\Omega]_{MM'}(r), \quad r > d_{MM'} \tag{2.3}$$

where

$$\Delta\mathrm{C}_{MM'}(r) \approx -\beta \mathrm{v}_{MM'}(r) g^{(0)}_{MM'}(r) \tag{2.4}$$

and the asterisks denote spatial convolutions. For site-site interaction potentials consisting of hard-core repulsive ($r < d_{MM'}$) and attractive tail ($r > d_{MM'}$) branches, $d_{MM'}$ is the distance of closest approach between the inpenetrable sites of species M and M′. These hard-core diameters characterize the athermal "reference system". The superscripts (0) denote the reference system correlation functions, determined here by the standard site-site Percus−Yevick (PY)[36,44] approximation:

$$C^{(0)}_{MM'}(r) = 0, \quad r > d_{MM'}$$

$$g^{(0)}_{MM'}(r) = 0, \quad r < d_{MM'} \tag{2.5}$$

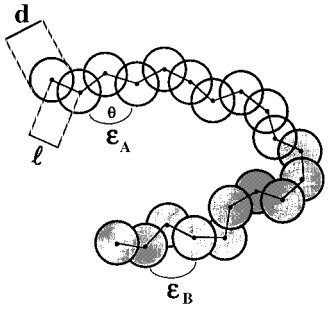

Figure 1. Schematic representation of the asymmetric semiflexible diblock model. The structure of any one block of species M is characterized by a bond length, l_M, a hard-core diameter d_M, and a local bending energy $E_{b,M} = \epsilon_{b,M}(1 + \cos\theta)$. Shown is the case for $d_A = d_B \equiv d$ and $l_A = l_B \equiv l$ which is used in this work.

While the full R-MPY closure ($\Delta C_{MM'}(r) \approx (1 - e^{+\beta v_{MM'}(r)}) g_{MM'}(r)$) accounts for the temperature-dependent structural correlations in the effective interactions ($C_{MM'}$), the above limiting HTA form approximates the packing correlations by their athermal values. Such a thermodynamic perturbative approximation is employed at the level of the renormalized potentials only and is not perturbative in $\beta v_{MM'}(r)$ for the quantities such as $g_{MM'}(r)$ and the collective structure factors. For the purpose of predicting apparent microphase separation temperatures based on extrapolation of the inverse peak collective structure factor, $1/S(k^*)$ vs $1/T$, the HTA is a natural and convenient choice. In this regime, the HTA is an accurate approximation to the full R-MPY closure. Detailed discussions and analysis of these closure approximations are given in refs 21, 24, and 43 for binary blends, and ref 20 for AB block copolymers. The Picard algorithm[44] was used to numerically solve the coupled nonlinear integral equations (three for AB copolymers) defined by eqs 2.2−2.5.

B. Asymmetric Diblock Model. There are many possible ways to model single chain structural asymmetries in diblocks and blends.[28,45] The simplest of these is a Gaussian model where the two species have different statistical segments lengths.[21,25,45] Stiffness asymmetries can also be modeled using a bond bending energy to impart local backbone stiffness in a more realistic finite hard core diameter semiflexible chain.[28] More sophisticated approaches would involve including side branches along the backbone to represent structural disparities in specific systems.[31,45,46] Interestingly, packing trends due to real structural disparities such as branching and variable torsional potentials can be quite realistically mimicked (in an average sense) using effective unbranched chains as discussed elsewhere.[28,45] In this case the chain model can be "calibrated" to correctly capture the monomer-averaged consequences of branching and variable aspect ratio on the local *inter*molecular packing properties of *one-component* melts.

As a continuation of the work presented in ref 28 on purely *athermal* stiffness asymmetric diblocks, we employ the discrete analog to the semiflexible wormlike chain.[47] A schematic representation of this model is shown in Figure 1, where for simplicity we have fixed the site hard-core diameters and the bond lengths to be equal, i.e. $d_A = d_B \equiv d$ and $l_A = l_B = l \equiv d/2$. The $l = d/2$ choice represents a reasonable value for mimicking the accessible surface area of a real repeat unit relative to its volume. Conformational stiffness mismatches enter solely through the pair of bond bending energies, $\epsilon_{b,A}$ and $\epsilon_{b,B}$. To characterize the degree of asymmetry in the chains we use species-dependent aspect ratios

$$\Gamma_M \equiv \sigma_M/d = \frac{\sqrt{6R_{g,M}{}^2/N_M}}{d} \approx \left(\frac{l}{d}\right)^2\left(\frac{2}{1+\langle\cos\theta\rangle_M} - 1\right) \tag{2.6}$$

where N_M is the number of sites of type M on a given chain. The average cosine of the angle formed by three consecutive sites of species M, $\langle\cos\theta\rangle_M$, is controlled by the bending energy $\epsilon_{b,M}$ (see ref 47 for details). Note that the last approximate equality in eq 2.6 is only rigorously valid for large N, but it is found to be accurate for shorter chains as well. The values of effective aspect ratio relevant to flexible chains (olefins, dienes, etc.) fall in the range $0.8 < \Gamma < 1.4$.[28,45] The reduced total site number density, $\rho_m d^3 = N\rho d^3$ ($N \equiv N_A + N_B$), is fixed at a value of 1.375, which results in an experimentally realistic dimensionless isothermal compressibility for the polyethylene-like pure melt model case of $\Gamma = 1.2$.[45]

C. Intermolecular Dispersion Interactions. Segments on different chains interact through pairwise decomposable hard-core repulsions for $r < d$, which enter the theory as the $g_{MM'}(r < d) = 0$ constraint (see eq 2.5), and a Lennard−Jones-like attractive tail for distances outside d

$$v_{MM'}(r) = \epsilon_{MM'}\left[\left(\frac{r}{d}\right)^{12} - 2\left(\frac{r}{d}\right)^{6}\right], \quad r > d \tag{2.7}$$

where the minimum has been shifted to $r = d$, and $\epsilon_{MM'} > 0$. Note that although the form of eq 2.7 contains two terms, it is defined to vanish for $r < d$, and it leads to purely attractive interactions. The (hard-core) repulsive interactions are manifest solely in the closure relation of eq 2.5. Dispersion interactions for nonpolar molecules are modeled in the simplest conceivable manner: by Bertholet scaling relations between the well depth parameters

$$\epsilon_{AA} \equiv \epsilon, \quad \epsilon_{BB} = \lambda^2\epsilon, \quad \epsilon_{AB} = \lambda\epsilon \tag{2.8}$$

Within simple Flory theory, the corresponding "bare" or mean field interaction parameter would have the form $\chi_o \propto \rho_m\beta\epsilon(\lambda - 1)^2$, where $\beta \equiv 1/k_BT$. This mean field interaction parameter neglects intermolecular packing correlations and corresponds to setting $g_{MM'}(r) = 1$ (random continuum). As a zeroth order, minimum parameter treatment of saturated hydrocarbon polymers with a common chemical repeat formula (e.g., C_4H_8) the parameter λ may be set to unity. This does *not* necessarily lead to a "cancellation" of the energetic driving force for segregation and a recovery of an athermal system (except in Flory theory where $\chi_o \to 0$), since the *effective* enthalpic interactions depend on packing-induced nonrandom mixing effects.[21] The miscibility behavior of the binary homopolymer blend analog of the above model has been recently studied using PRISM theory by Singh and Schweizer.[32]

III. Small-Angle Scattering

In compressible diblock fluids there are three unique, but related, partial collective structure factors defined by

$$\hat{S}_{MM'}(k) \equiv \int d(\mathbf{r} - \mathbf{r}')\, e^{i\mathbf{k}(\mathbf{r}-\mathbf{r}')} \langle [\rho_M(\mathbf{r}) - \rho_M][\rho_{M'}(\mathbf{r}') - \rho_{M'}] \rangle = \hat{\Omega}_{MM'} + \hat{H}_{MM'} \quad (3.1)$$

where the pointed brackets denote an ensemble average and $\rho_M(\mathbf{r})$ is the microscopic number density of species M at point $\mathbf{r}$. The long wavelength collective structure factors provide indicators of the proximity to the microphase separation boundaries, and deviations from the incompressible relation $\hat{S}_{AA}(k) = \hat{S}_{BB}(k) = -\hat{S}_{AB}(k)$ quantify structural and interaction asymmetry effects.

Shown in Figure 2 is a typical example of the temperature dependence of the scaled reciprocal peak intensities, $N/\hat{S}_{MM'}(k = k^*)$, for N = 2000 with $\Gamma_f = 1$, $\Gamma_s = 5/4$, $f = 0.5$, and $\lambda = 1$. Here "s" and "f" refer to the "stiff" and "flexible" components. At high temperatures a linear, mean-field-like, dependence is found. Fluctuations in concentration which develop at lower temperatures give rise to stabilizing nonlinearities. These effects are also present in simpler structurally symmetric models within the present theory,[20] as well as field theories which account for fluctuation effects,[11,13] and seem to be a generic feature of most experimental systems provided the low-temperature melt is accessible. Note, however, that a distinction between the scattering from stiff and flexible components can only be made within a theory for compressible liquids.

The range in $1/T$ relevant to many real experiments and the extraction of an apparent microphase spinodal is shown in the main part of Figure 2. We have defined the "apparent spinodal" temperature in the usual way, as indicated by the dashed lines. Of course, this is *not* expected to be precisely the ODT temperature, but it is correlated with such a quantity.[48,49] In the following sections we examine the "microphase stability" and the low-temperature liquid structure, and our definition of $T_{s,app}$ serves as an indicator of the proximity to the true microphase separation transition occuring at T_{ODT}. Note that regardless of the differences between the three partial structure factors, the extrapolation of their high-temperature parts converge to a single point, yielding a unique $T_{s,app}$.

What may differ from system to system is the detailed shape of the reciprocal peak intensity vs $1/T$. Figure 3 shows the collective scattering curves over a very wide temperature interval, normalized to their respective athermal values, for the common "A" block ($\Gamma_A = 1$) in a series of $N = 2000$, $f = 0.5$ diblocks with structural asymmetries of $\gamma \equiv \Gamma_B/\Gamma_A = {}^4/_5$, ${}^5/_4$, and ${}^3/_2$ and $\lambda = 1$. The curvature and/or the degree to which nonlinearities exist at given temperature seems to be sensitive to the nonuniversal asymmetries in structure. In particular, both negative and positive curvatures at intermediate temperatures are possible. These subtle, system specific curvature effects are difficult to interpret due to simplifications adopted which would quantitatively influence the predicted intermediate temperature behavior. For example, "equation of state" effects in the reference system (allowing the density, and perhaps aspect ratios, to change as a function of temperature, consistent with a constant pressure condition) have been ignored. If included, then lower temperatures would lead to a higher reduced density $\rho_m d^3$ and hence a larger value of $-\rho_m \hat{C}_{MM'}(k = 0)$ which is inversely proportional to the isothermal compressibility of the liquid. This would keep the relative magnitude of the repulsive force contribution to $\hat{C}_{MM'}(k)$ larger than the temperature-dependent attractive interaction correction and guarantee the physically sensible trend of decreasing compressibility upon cooling. Thus, the two primary factors which appear to influence the magnitude of both the negative and positive curvatures in this model study are compressibility effects and the relative and absolute magnitudes of the block aspect ratios. We have found that copolymers with larger aspect ratio disparity and/or a large overall (average) aspect ratio tend to exhibit the least amount of curvature. For all of the aspect ratios studied, the larger chains (as shown in Figure 3) show extremely small negative curvatures. On the other hand, for short chains ($N \approx 100$, not shown) and/or small structural disparity ($\gamma \approx 1$), the negative curvature effects are more dramatic. Since we are focusing on longer chains in this study (and in our applications to the polyolefin diblock melts), we have not characterized these curvature effects quantitatively.

When viewing Figure 3, it is important to realize that real experiments cover only some *finite* range in inverse temperature and thus may not show appreciable deviations from linearity at the highest accessible temperature (as in Figure 2). That is, over the temperature window in which the measurements are often made (usually in the fluctuating regime near the ODT), we

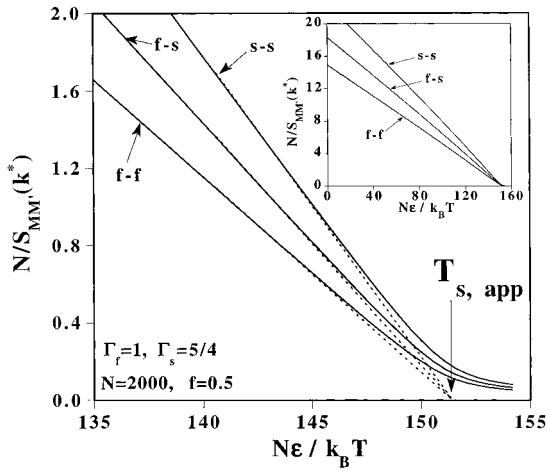

Figure 2. Reciprocal peak scattering intensity for an asymmetric diblock melt with $N = 2000$, $f = 0.5$, $\Gamma_s = {}^5/_4$, and $\Gamma_f = 1$. As discussed in the context of athermal systems,[28] the flexible component is less stable to microdomain-scale fluctuations, and hence has a larger $\hat{S}(k^*)$. Shown also as dotted lines are the high temperature extrapolations. These converge to a unique apparent spinodal temperature.

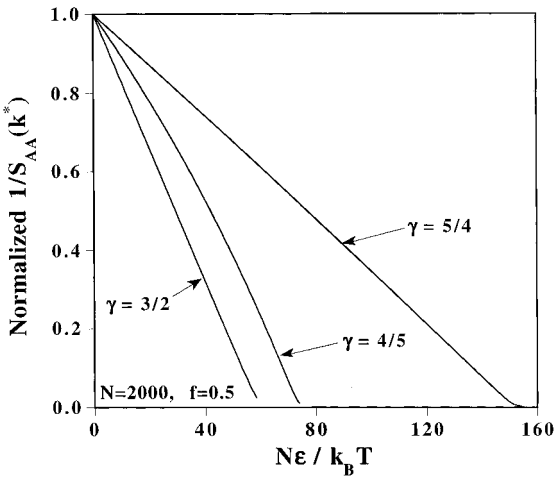

Figure 3. Common block reciprocal scattering intensity (normalized to unity) for a common block aspect ratio of $\Gamma_A = 1$ and variable block aspect ratios of $\Gamma_B = 4/5$, $5/4$, and $3/2$. Shown are the cases for $\lambda = 1$, $N = 2000$, and $f = 0.5$.

do not expect strong curvatures to be observed on the high temperature side. Regardless of the details of *how* the system approaches the apparent spinodal from high temperature, the theory ultimately predicts a stabilization at low temperatures indicated by a positive curvature in $\hat{S}_{MM'}^{-1}(k^*)$ vs $1/T$, as in the symmetric model cases studied previously.[20] A lower magnitude of a given curve (at constant T) indicates a melt closer to its $T_{s,app}$. For modest block stiffness differences, the change in $T_{s,app}$ is a numerical factor related to the absolute and relative magnitudes of the block aspect ratios Γ_M (see section IV below). In general, the local nonrandom packing effects and energetics are coupled, and therefore the sensitivity of the scattering curves to conformational asymmetries will vary with different combinations of structural and interaction asymmetry (λ parameter).

The inverse peak intensities exhibit the least amount of stabilizing curvature when a large degree of structural asymmetry exists. The $\gamma = \Gamma_B/\Gamma_A = 3/2$ case in Figure 3 corresponds to the stiffest diblock (in an average aspect ratio sense) and hence has the smallest amplitude of long wavelength total density fluctuations or compressibility. On the basis of prior analytic PRISM work,[20,49] the correlated enthalpic feedback process for fluctuation stabilization is expected to be weakened as the fluid becomes more incompressible, in qualitative accord with the trends seen in Figure 3.

It has previously been shown within the context of binary polymer blends and block copolymers[20,21] that the so-called assumption of "effective incompressibility" leads to simplified relations between the partial structure factors. "Effective incompressibility" is defined as the small wave vector condition $-\hat{\Omega}_{MM'}(k)\hat{C}_{MM'}(k) \gg 1$, leading to the following scaling relations between the three partial structure factors:

$$\hat{S}_{BB}(k) \approx \frac{\hat{C}_{AA}(k)}{\hat{C}_{BB}(k)}\hat{S}_{AA}(k) \tag{3.2}$$

$$\hat{S}_{AB}(k) \approx -\frac{\hat{C}_{AB}(k)}{\hat{C}_{BB}(k)}\hat{S}_{AA}(k) \tag{3.3}$$

For athermal Gaussian thread polymers, the large N limit reduces these ratios of direct correlation functions to $C_{BB}^{(0)}/\hat{C}_{AA}^{(0)} = \gamma^4$ and $C_{AB}^{(0)}/\hat{C}_{AA}^{(0)} = \gamma^2$, where $\gamma \equiv \Gamma_B/\Gamma_A$.[21,50] Although we do not expect these simple relations involving γ to hold quantitatively for finite hard core diameter semiflexible chains at finite temperature, it is of interest to study numerically the degree to which eqs 3.2 and 3.3 do hold.

Shown in Figure 4 are the ratios of the $k = k^*$ partial structure factors and direct correlation functions for $N = 2000$, $f = 0.5$, with $\Gamma_s = 1$, $\Gamma_f = 4/5$, and $\lambda = 1$. At this meltlike density and large N value, the scaling relations of eqs 3.2 and 3.3 appear to hold quite well throughout the entire temperature range. Calculating the athermal thread limit prediction, we find that the scaling in terms of the stiffness asymmetry parameter γ quantitatively overestimates the ratios but does reasonably well considering the highly coarse grained nature of the Gaussian thread model.

IV. Extrapolated Microphase Separation Spinodals: General Trends

Analytical calculations using the idealized Gaussian thread model[21] within the R-MPY/HTA closure approximation predict competing effects between the local

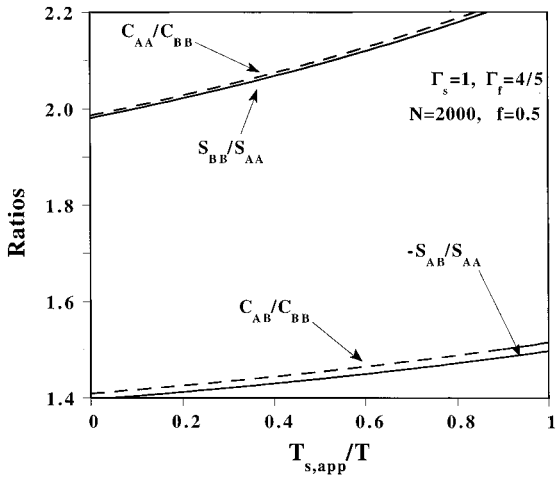

Figure 4. Temperature dependence of direct correlation function and partial structure factor ratios evaluated at the peak scattering wave vector k^*.

conformational (stiffness) and chemical interaction mismatch. The microphase separation spinodal temperature,[21] which is rigorously predicted (not based on extrapolation) by PRISM theory in the idealized Gaussian (fully flexible) thread ($d \to 0$) model limit, is given by[51]

$$\frac{k_B T_s}{\rho_m \tilde{H}} = f(1-f)(\lambda - \gamma^2)^2 F(k^*, f, \gamma)N + (-\rho_m C_{AA}^{(0)})^{-1} G(k^*, f, \gamma, \lambda) \tag{4.1}$$

where

$$NF(k) = \frac{\hat{\omega}_{AA}(k)\hat{\omega}_{BB}(k) - [f(1-f)]^{-1}\hat{\omega}_{AB}^2(k)}{f\hat{\omega}_{AA}(k) + \gamma^4(1-f)\hat{\omega}_{BB}(k) + 2\gamma^2\hat{\omega}_{AB}(k)} \tag{4.2}$$

$$G(k) = \frac{f\hat{\omega}_{AA}(k) + \lambda^2(1-f)\hat{\omega}_{BB}(k) + 2\lambda\hat{\omega}_{AB}(k)}{f\hat{\omega}_{AA}(k) + \gamma^4(1-f)\hat{\omega}_{BB}(k) + 2\gamma^2\hat{\omega}_{AB}(k)} \tag{4.3}$$

and k^* is defined as the value of k which maximizes T_s. For the thread model, $\tilde{H} \equiv |\hat{v}_{AA}(0)|a/(a + \xi_{eff})$, where a is the spatial range of the (Yukawa) attractive interactions, and ξ_{eff} is a composition- and γ-dependent effective density fluctuation screening length (see ref 21 for details). Here, the intramolecular structure factors are related to those introduced earlier through $\hat{\omega}_{MM}(k) \equiv \rho_M^{-1}\hat{\Omega}_{MM}(k)$ and $\hat{\omega}_{AB}(k) \equiv \rho_m^{-1}\hat{\Omega}_{AB}(k)$. If γ, $\tilde{H}$, and ρ_m are taken as temperature independent, then the first term obeys the classical scaling law of $T_s \propto N^1$, while the second term represents an N^0 compressibility correction. Equation 4.1 is very similar to the expression for T_s in a binary polymer blend[21] of composition ϕ, given by

$$\frac{k_B T_s}{\rho_m \tilde{H}} = \frac{(\lambda - \gamma^2)^2}{\phi + \gamma^4(1-\phi)}\phi(1-\phi)N \tag{4.4}$$

where we have dropped the N^0 compressibility term.

Although for finite thickness ($d \neq 0$) semiflexible chains only a numerically determined (extrapolated) *apparent* spinodal exists, it is interesting to see how closely the present more realistic model follows the analytical thread model predictions. First, to emphasize the importance of cross terms between structural cor-

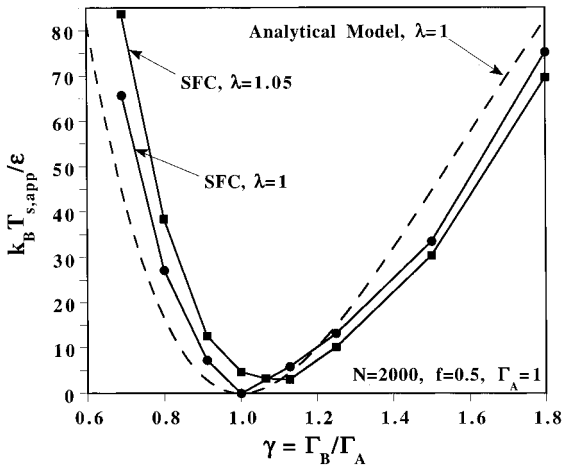

Figure 5. Apparent spinodal phase diagram for $N = 2000$ stiffness asymmetric diblock copolymer melt at $f = 0.5$. Here $\Gamma_A = 1$, while Γ_B was varied. Circle points are for when all bare attractive interactions are identical $\lambda = 1$, squares are for $\lambda = 1.05$. Note that the (mean-field) "critical point" for each stiffness ratio is *not* necessarily at $f = 0.5$. The analytical thread model prediction of eq 4.1 is also shown as the dashed curve for the $\lambda = 1$ case.

relations and interactions, we have calculated the apparent microphase separation spinodal phase diagram for the $\lambda = 1$ case, where the bare Flory χ-parameter $\chi_o \equiv 0$. Figure 5 shows the constant density predictions for the dependence $T_{s,app}$ on the conformational asymmetry variable $\gamma \equiv \Gamma_B/\Gamma_A$ for a diblock melt with $N = 2000$, $f = 0.5$, and a common block aspect ratio of $\Gamma_A = 1$. Of course, when $\gamma = \lambda = 1$ this becomes a homopolymer melt, and hence the $k = k^*$ apparent spinodal disappears. The apparent spinodal temperature monotonically increases as the variable block becomes either stiffer or more flexible than the common block ($\gamma > 1$ and $\gamma < 1$, respectively). However, the effect is not symmetric about $\gamma = 1$, as we expect the *average* copolymer stiffness ($2\bar{\Gamma} \equiv \Gamma_A + \Gamma_B$) to affect $T_{s,app}$ as well. This general behavior is also predicted by the analytical thread model, as seen by the dashed curve in Figure 5. Here, we used eq 4.1, and fit to the overall temperature scale of the numerical finite hard core calculations by using $\hat{v}_{AA}(0)$ (the "bare" potential energy well depth in the analytical model). Our primary interest is whether the relative trend predicted by the analytical model is an accurate representation of the more realistic finite hard core results. We also performed (not shown) this procedure using the simpler analytical blend result of eq 4.4. The shape of the resulting blend curve is very similar to the dashed curve in Figure 5 coming from eq 4.1. Thus, not only does the analytical model for diblocks faithfully represent the general behavior seen in the more realistic finite hard core calculations, the *blend* formula of eq 4.4 also appears to be a reasonable approximation for the long diblock.

Figure 5 also shows the numerical predictions for $\lambda = 1.05$ representing a small degree of bare chemical interaction asymmetry. This value of λ is appropriate for describing the bare energetic differences between PE, PEP, and PEE based on either solubility parameter or van der Waals attractive constant schemes.[45] Although the general features of the $\lambda = 1$ and $\lambda = 1.05$ diagrams are the same, the latter case leads to a shift of the minimum, or "most stable" point, to higher γ. This trend is also consistent with the analytical thread predictions of eqs 4.1 and 4.4, and represents the tendency for chemical and structural mismatches to "cancel" or "compensate" if $\gamma, \lambda > 1$, but "reinforce" if $\lambda > 1$ and $\gamma < 1$.[21] Strong evidence to support the existence of such subtle effects is present in so-called "deuteration swap" experiments.[2,3] This nonadditivity of packing and enthalpic effects and the connection to such swap experiments have been discussed by Singh and Schweizer.[32]

Table 1. Effect of Changing Block Aspect Ratio on Microphase Spinodal Instabilities for $\lambda = 1$[a]

	$R \equiv T_{s,1}/T_{s,2}$		
$\Gamma_{B,1}/\Gamma_{B,2}$	SFC	thread	$(\gamma^2 - \lambda)^2/(1 + \gamma^4)$
0.69/0.8	2.42	2.69	2.41
1.5/1.25	2.54	2.98	2.80
1.8/1.25	5.70	5.53	4.76
1.8/1.5	2.25	1.86	1.70
0.8/1.25	2.05	1.10	1.00
1.5/0.8	1.24	2.70	2.80
1.8/0.8	2.77	5.01	4.76

[a] Listed are the changes in the apparent spinodal temperatures upon changing the variable block aspect ratio, Γ_B for $N = 2000$. The common stiffness block has $\Gamma_A = 1$. The "SFC" column contains the numerical finite hard core predictions; the "Thread" column shows the results based on eq 4.1.

In Table 1 the ratio of apparent spinodal temperatures upon changing the variable block aspect ratio is given for several cases. For example, when Γ_B is changed from 1.25 to 1.5 (second row in Table 1), $T_{s,app}$ is changed by a factor of roughly 2.5. The trends predicted by the thread model are consistent with the numerics *within* a given branch (the first four entries in the table) of the spinodal phase diagram (i.e. $\gamma < 1$ or $\gamma > 1$). On the other hand, changes of the variable block which result in crossing over $\gamma = 1$ (the bottom three entries) are not as well described by the analytical formula. Nonetheless, the *direction* of the changes is correctly captured by the thread model for all of the cases.

Part A of Figure 6 shows predictions for the copolymer composition dependence of $T_{s,app}$ for $\lambda = 1$ and $N = 2000$. Two different values of structural asymmetry are shown, one representing a fairly flexible copolymer with $\Gamma_B/\Gamma_A = 0.8/1.0$ and the other having $\Gamma_B/\Gamma_A = 1.5/1.0$, characteristic of a more rigid diblock. For compositions spanning a region about the compositionally symmetric $f = 0.5$ case, the copolymer with a larger stiffness asymmetry reaches the apparent spinodal at a higher temperature. On physical grounds, this seems reasonable, as stiff−flexible polymers might be expected to more easily segregate due to the packing constraints. However, at the extreme compositions the phase behavior looks to be determined by the overall, or average, stiffness of the polymer. The more flexible (and hence more compressible within our present constant volume, not pressure, model) system is predicted to have a higher $T_{s,app}$ near the one-component polymer limit. This crossover effect is likely tied to the fact that a $k = 0$ instability becomes the *only* transition present in the $f = 0$ and $f = 1$ limits, and hence compressibility effects become important. This point is more easily illustrated with the Gaussian thread model result of eq 4.1. To look at the relative importance of compressibility effects (i.e. the second term in eq 4.1), we have plotted results of eq 4.1 for T_s/N in part B of Figure 6. Note that the compressibility term scales as N^0 and represents a $k = 0$ spinodal instability. We have shown T_s/N, and hence the *relative* effect of this N^0 term is seen to be much larger for the finite N. The crossing of the low and high

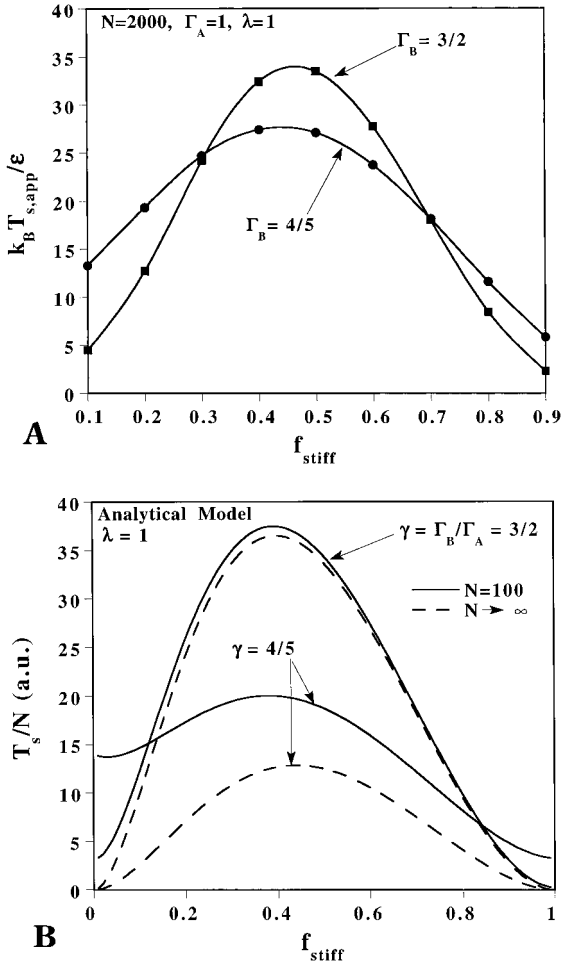

Figure 6. (A) Numerical predictions of composition dependence of $T_{s,app}$ for $N = 2000$ and $\lambda = 1$ based on the model depicted in Figure 1. The stiffness asymmetries are $\Gamma_B/\Gamma_A = 0.8/1$ and $\Gamma_B/\Gamma_A = 1.5/1$. The points are the calculated values and the lines are guides to the eye. (B) Analytical predictions for microphase spinodal temperatures comparing finite N to $N \rightarrow \infty$. Here $\lambda = 1$, and the structural disparities are the same as in part A.

stiffness cases seen in Figure 6A appears to be qualitatively captured in the thread calculation of Figure 6B. That is, the competition between compressibility effects and the $k \neq 0$ microphase separation spinodal instability leads to a reversal in the trend of T_s with copolymer stiffness near the compositional edges of the spinodal phase diagram. Note, however, the analytic thread model predicts a much stronger dependence of T_s on γ than found in the numerical results due to its oversimplified fully flexible and vanishingly thin ($d \rightarrow 0$) nature.

V. Application to Polyolefin Diblock Copolymer Experiments

The general trends discussed in section IV should apply to polymers within the range of aspect ratios relevant to the olefins, dienes, and other flexible copolymers which are composed of monomers having modest chemical disparity ($\lambda \approx 1 \pm 0.05$). Further, the same trends seem to hold for levels of single-chain description ranging from the Gaussian thread to the semiflexible finite hard core diameter chain, as seen in Figures 5 and 6. What *will* be more sensitive to the choice of model is the absolute temperature scale on which the apparent phase boundary lies. Once this is determined, the relative ordering of the spinodal temperatures is expected to obey the same general trend with conformational and interaction asymmetry as discussed above.

Table 2. Parameters Used in the Comparison to Experiment[45] [a]

	calculation parameters					
mapping	Γ_{PE}	Γ_{PEP}	Γ_{PEE}	$S_{o,PE}(0)$	$\rho_m d^3$	ϵ/k_B, K
1	1.2	1.12	1.0	0.254	1.375	48.69
2	1.0	0.952	0.898	0.254	1.6303	57.80

[a] Listed are the block aspect ratios Γ_M, liquid density $\rho_m d^3$, and associated dimensionless compressibility $S_{0,PE}(k = 0)$. For each mapping the density was chosen by requiring that the dimensionless compressibility of a pure PE melt (for the model aspect ratio) was reproduced (see section V).

A. Microphase Separation Temperatures. Here, we present a "zeroth order" treatment of a minimalist model for polyolefin phase behavior, in order to examine the ability of the theory to predict the absolute magnitude of the transition temperatures and degree of polymerization and microstructural trends found in recent experiments by Bates and co-workers.[1,5] The aspect ratios of flexible polyolefins and estimates for such quantities based on an equal monomer volume basis appropriate for our model have been presented elsewhere.[45] Because we expect the dispersion interactions amongst the olefinic polymers to be very similar, we use a minimal parameter estimate for the ordering of attractive well depths of $\lambda = 1$, corresponding to a mean field Flory χ-parameter of *identically zero*. Thus the absolute magnitude of the well depth, ϵ, is the only freely adjustable parameter.

We have performed two series of calculations corresponding to different "mappings" (effective aspect ratio choice) of the real branched polymers to unbranched effective homopolymer chains. The system parameters of both mappings are listed in Table 2 and are consistent with direct estimates based on known monomer volumes and characteristic ratios, as well as the relative values of *melt* solubility parameters.[45] For each mapping ϵ/k_B was fit to the single PE/PEE data point[1] for $N_{seg} = 410$,[52] and the same value was employed to make predictions for the other systems and degrees of polymerization. Note that in reality T_{ODT} is not expected to precisely coincide with $T_{s,app}$.[1,5,49] In this zeroth-order treatment, we have assumed the difference between the two temperatures (although not truly a constant) to be absorbed into the fitted well depth. The magnitudes of the fitted well depths for the two mappings are reasonable when compared to *ab initio* estimates of the interactions between methylene groups of $\epsilon/k_B \approx 40-60$ K.[38,53] This is a very important feature supporting our basic premise that the fundamental driving force for polyolefin microphase separation is local enthalpic interactions modified by conformational asymmetry induced packing differences. In each mapping we chose the density such that the PE melt dimensionless compressiblity at $T = 430$ K was reproduced.[45,54] This initial calibration of the fluid density does not depend on copolymer data, and is a procedure meant to introduce a realistic compressibility based on single-component melt data.

Figure 7 shows the resulting apparent spinodal temperatures, along with the ODT temperatures of Bates et al.[1,5] We again emphasize that our comparison is *not* a set of fits; only the $N_{seg} = 410$ data point for PE/PEE was fit by varying the energy scale parameter ϵ. It is encouraging that at the current level of description, the correct *trend* with stiffness asymmetry seems to be captured, regardless of mapping. This trend can also be reproduced using the analytical thread model,[21] suggesting that the monomer-structure-dependent

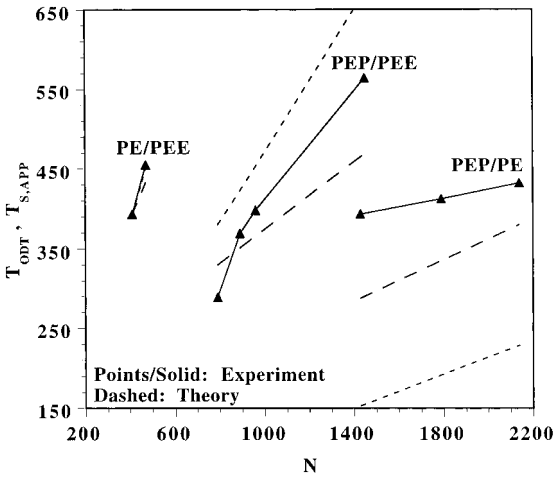

Figure 7. Comparison with experimental ODT temperatures for polyolefin diblocks. Shown are the experimental order-disorder transition temperatures of Bates et al.[1,5] and our predicted *apparent* spinodal temperatures. The short and long dashes are for "mappings" 1 and 2, respectively. In the figure, N is the number of segments (not sites) as defined in ref 1.

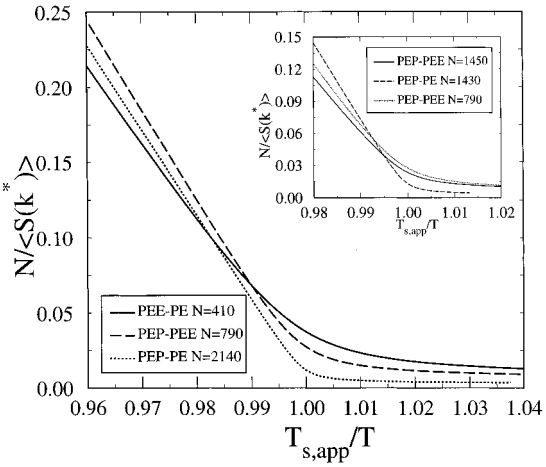

Figure 8. Reciprocal small-angle peak scattering intensities[55] for selected chain lengths in the model application to PEP−PE, PEP−PEE, PEP−PE systems. The main part of the figure shows plots for PEE−PE, $N = 410$; PEP−PE, $N = 790$; and PEP−PE, $N = 2140$. This portion of the figure shows the general trend of smaller fluctuation effects for larger N. The inset displays plots for PEP−PEE, $N = 1450$; PEP−PE, $N = 1430$; and PEP−PEE, $N = 790$. For the two cases of nearly the same N, the system having the lower average aspect ratio (PEP−PEE), and hence larger compressibility, has stronger non-mean-field effects.

changes in the slopes of the transition temperature can be predicted using fairly simple unbranched, effective stiffness, chain models. The key feature in the theory giving rise to such predictions is that increasing chain aspect ratio results in tighter local intermolecular packing, which in turn enhances the cohesive energy density associated with the dispersion interactions.[45]. We also note that the absolute magnitudes of our predictions are quite sensitive to choice (mapping) of Γ_M. Even in the case of PEP/PE, if we allow for small changes in $\gamma \equiv \Gamma_{PEP}/\Gamma_{PE}$, then the slope and magnitude can be closer to experiment than our predictions of Figure 7 in which no additional parameters (beyond the microscopic well depth for PE/PEE $N_{seg} = 410$) were fit. The unusually weak dependence of T_{ODT} on N for PEP/PE is also observed for the analagous binary blend,[1] and thus does not appear to be a concentration fluctuation related effect.

Obviously there are many refinements which can be introduced in this approach, which may result in more quantitative agreement even within our SFC model. These include accounting for the temperature dependence of the chain dimensions and density, accounting for the differences in polarizability between CH, CH_2, and CH_3 subunits (i.e. $\lambda \neq 1$ and hence $\chi_o \neq 0$), and explicit treatment of the branches.[31,46]

B. Concentration Fluctuation Stabilization. The apparent spinodal temperatures do not carry any information about the role of concentration fluctuations (beyond the relatively low amplitude fluctuations present in the athermal system resulting from nonrandom packing of structurally asymmetric chains[28]) since $T_{s,app}$ is defined as an extrapolation of the higher temperature, linear portion of the $S^{-1}(k^*)$ vs $1/T$ curve. Since the concentration fluctuation stabilization mechanism in PRISM theory is driven by a coupled enthalpy-induced local clustering of like monomers process, it is quantitatively sensitive to nonuniversal features such as block aspect ratios, liquid density and compressibility, and spatial range of the attractive tail potentials[20] in a manner which *cannot* be reduced to a renormalized parameter $\bar{N} = N(\rho_m\sigma^3)^2$ as found using coarse-grained BLFH theory for Gaussian thread chains. In addition, since the PRISM stabilization mechanism is a finite N effect, more mean-field-like behavior is predicted as the degree of polymerization of the chain is increased *if* all other relevant physical factors are held constant. This sensitivity of the quantitative efficiency of the feedback stabilization process to multiple system variables, and mapping of the real copolymer onto our SFC model, suggests complicated behavior may emerge for some experimental systems.

To address the above issues, we show in Figure 8 representative results for the (species-averaged[55]) inverse small-angle peak scattering intensities as a function of reduced inverse temperature near the extrapolated spinodal. The main portion of Figure 8 shows results for three different polyolefin materials at three different chain lengths. For the chosen cases, it is clear that as N increases the nonlinear fluctuation regime narrows as expected for a finite size stabilization process. This agrees qualitatively with recent polyolefin experiments.[5]

A more quantitative characterization of the width of the fluctuation stabilization regime can be obtained by empirically defining a second temperature, $T_{ODT,app}$, as the temperature at which a linear extrapolation of the tangent line to the curve at $T_{s,app}$ crosses the $\hat{S}^{-1}(k^*) = 0$ axis. Guenza and Schweizer[49] have argued elsewhere that this empirical definition seems to be a remarkably good estimate of the true ODT temperature for real experimental data, as well as for the BLFH theory ODT temperature. For the cases in Figure 8, the ratio $r = T_{s,app}/T_{ODT,app} = 1.018$(PE/PEE), 1.012(PEP/PEE), 1.005(PEP/PE). There are two important features of these numbers: (1) The shift parameter, $\Delta \equiv r - 1$, is in the range of 0.5−2 %. This appears to be smaller than experimental results for N in the range of 400−2000 where $\Delta \approx 1-10\%$.[1,5] However, such quantitative differences in the absolute magnitudes is not unexpected for several reasons. These include (a) the ambiguity of what absolute values of N and melt density to assign our finite thickness SFC chain model (discussed in the opening paragraph of this subsection) for a particular experimental sample (with PRISM theory an atomistic model is required to completely avoid this issue), and

(b) the R-MPY/HTA closure employed in this paper does not contain all the feedback mechanisms present in the R-MPY closure previously studied[20,49] and hence is expected to *under*estimate the magnitude of the fluctuation stabilization process. Quantitative fitting of the simple analytical thread model version of diblock copolymer PRISM theory[20] based on the full R-MPY closure to scattering data is given elsewhere;[49] excellent agreement is found even with regard to the absolute magnitudes of the width of the fluctuation regime. (2) The shift parameter Δ decreases even more strongly than the $N^{-1/3}$ law anticipated by both PRISM/R-MPY[20] and BLFH[11] theories. This subtle behavior may reflect the influence of copolymer mean aspect ratio which increases going from PEE−PEP to PEE−PE to PEP−PE, thereby reducing concentration fluctuation stabilization.

The cases shown in the main part of Figure 8 suggest the influence of N on the feedback process is the primary factor in determining the qualitative trends. However, within a more narrow range of chain lengths, nonuniversal competing effects can lead to a more complex N dependence in such plots. An example of this is shown in the inset of Figure 8. At a nearly fixed N of 1450, the higher aspect ratio (less compressible) PEP/PE diblock shows a significantly smaller fluctuation stabilization region than the "more flexible" (and hence more compressible liquid) PEP/PEE diblock. This clearly demonstrates the effect described above of fluctuation stabilization suppression for "better packing" (higher aspect ratio) diblock chains. On the other hand, changing N from 790 to 1450 for PEP/PEE does not significantly suppress the concentration fluctuation regime. Rather, very little change is seen. Similar behavior (not shown) is found for the PEP/PE and PE/PEE cases, i.e. weak dependence of Δ on N over modest changes in degrees of polymerization studied for each chemical structure. The origin of such subtle behavior may be due to our use of a constant volume model for which the melt compressibility generally increases with increasing N. The latter effect tends to enhance the fluctuation stabilization process and thus (partially) compensates for the reduction of finite size coupling of local and microdomain correlations for longer chains.

VI. Thermally Induced Packing Modifications

A. Radial Distribution Functions. There are three distinct intermolecular site-site radial distribution functions for the conformationally asymmetric AB copolymer. Nonrandom packing in the athermal limit leads to the intuitively sensible general trend in the ordering of the *local* correlations as follows:

$$g_{ss}(r) > g_{fs}(r) > g_{ff}(r) \qquad \text{athermal} \qquad (6.1)$$

An example of this is shown in Figure 9A. This ordering is a consequence of the better packing, or "layering" efficiency, of the stiffer, more open chains which experience more intermolecular contacts and hence enhanced solvation-shell-like structure. However, these athermal correlations do *not* lead to large microdomain scale ($\approx 2\pi/k^*$) collective fluctuations.[28] This is dramatically shown by the extremely low amplitude of the "pairing" or "clustering" function $2\Delta g(r) \equiv g_{AA}(r) + g_{BB}(r) - 2g_{AB}(r)$ in the inset of Figure 9A.

The *athermal* trends depicted in Figure 9A are modified by enthalpy-induced intermolecular segregation. In previous studies of symmetric diblocks,[20] we showed that the presence of intermolecular tail potentials leads to strong local clustering of like species and a marked depletion of A−B contacts. The magnitude of this effect near the apparent spinodal temperature is also consistent with recent computer simulations.[34,35] At fixed thermodynamic state, such clustering is enhanced as N and/or the copolymer (solution) density decreases.[20] In the context of the conformationally asymmetric diblocks, we expect qualitatively similar trends with the addition of attractive tail interactions but with quantitative nonuniversal deviations.

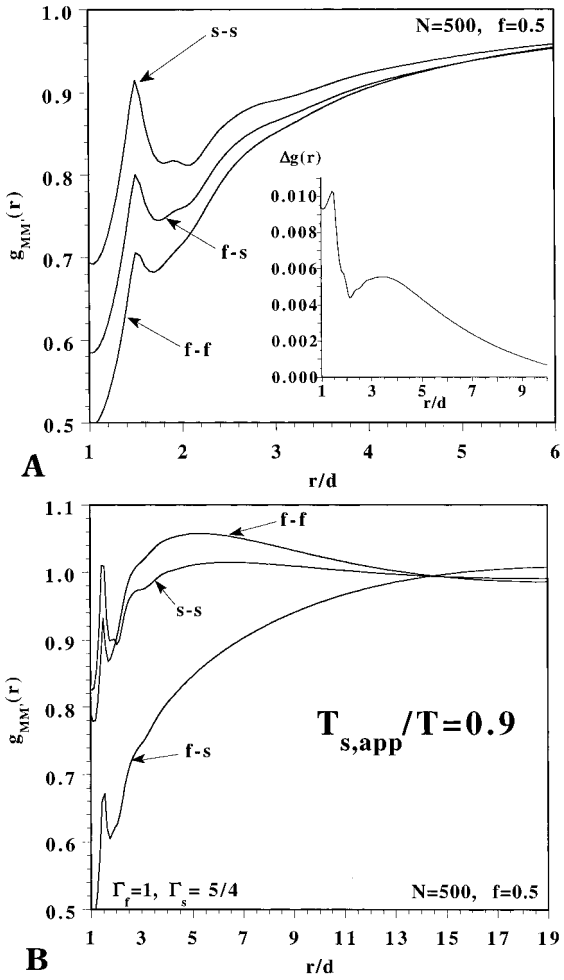

Figure 9. (A) Athermal radial distribution functions for an $N = 500$, $f = 0.5$ asymmetric diblock melt with $\Gamma_s = {}^5/_4$ and $\Gamma_f = 1$. The difference function $\Delta g(r)$ is plotted in the inset for comparison to the magnitude of $\Delta g(r)$ in the thermally interacting case shown in Figure 10. (B) Low-temperature radial distribution functions for an $N = 500$, $f = 0.5$ asymmetric diblock melt with $\Gamma_s = {}^5/_4$ and $\Gamma_f = 1$.

Shown in Figure 9B is an example of the low temperature pair distribution functions for the same system as in Figure 9A. In contrast to the trend of eq 6.1 seen in Figure 9A, the enthalpic interactions lead to a substantial modification of the local packing. First note that there is a general similarity between Figure 9B and the low temperature pair distribution functions of the *symmetric* model discussed previously.[20,28] This is seen as a large depletion of intermolecular flexible−stiff contacts, consistent with the expectation that segregation occurs at lower temperatures, and diffuse interfaces develop. Along with this depletion of unlike species contacts, an appreciable enhancement over the athermal values is predicted for contacts between like species. Moreover, the spatial range of the nonrandom packing persist to distances much larger than the local repeat unit length scale. Such long wavelength oscillations are

expected for diblock copolymers as the fluid approaches a microphase-separated state. These similarities in the low-temperature structural correlations in symmetric and asymmetric fluids arise from the same physical mechanism: the coupling of the local enthalpic interactions with intermolecular fluid structure.[20]

However, the precise models in the structurally symmetric vs asymmetric cases are very different. The structurally and interaction symmetric model previously studied analytically and numerically is by definition a homopolymer melt in the athermal limit, and hence there is perfect random mixing (i.e. $g_{MM'} = g$). Thus intermolecular segregation is driven exclusively by the unfavorable A−B tail interaction. In the conformationally asymmetric case presented here, there are *weak* concentration fluctuations in the athermal limit, and all species interact through *attractive* van der Waals forces. In fact, for this particular calculation all tail interactions were taken to be identical ($\lambda = 1$). The fact that *any* segregation takes place in this system dramatically highlights the importance of local packing-driven correlation effects associated with the block conformational asymmetry. What is remarkable is that the *magnitudes* of the induced structural modifications in the two very different systems appear to be similar near their respective apparent spinodal temperatures. Thus, the idealized structurally symmetric model containing only a repulsive A−B tail interaction seems to capture well the *general* clustering phenomenon predicted for more realistic model systems.

Also noteworthy is the difference in the trends with block stiffness between the athermal pair distribution functions of parts A and B of Figure 9. Whereas for pure packing reasons, the stiff−stiff correlations are largest in the athermal limit, Figure 9B suggests that the flexible−flexible correlations change more with temperature, and eventually can become larger in magnitude with respect to g_{ss} on intermediate length scales ($r \geq 2d$ for the example shown). Of course, *very locally* the ordering can vary and is model dependent. For the example in part B of Figure 9, $g_{ss}(r) > g_{ff}(r)$ for $r < 2d$ corresponding to a dominance of athermal "density-fluctuation-like" effects at very short distances. This trend reverses at larger r due to the enhanced long wavelength concentration-like fluctuations displayed by the more flexible component (see Figure 2). The overall stability against microphase separation of the flexible component is lower [$\hat{S}_{ff}(k^*) > \hat{S}_{ss}(k^*)$], and hence its intermolecular structure is more easily modified by the presence of unfavorable effective interactions. This is akin to the homopolymer case, where packing modifications for more compressible, or more loosely packed, fluids are more dramatic with changes in temperature or chain length at fixed density.

To contrast the degree of nonrandom mixing in the low temperature fluid to that of the athermal case (see the inset of Figure 9A), $\Delta g(r)$ is plotted in Figure 10 for the same system. We have also shown $\Delta g(r)$ for a more flexible copolymer with $\Gamma_s = 1$, $\Gamma_f = 4/5$. In both cases the magnitude of the pairing amplitude at low temperatures is more than an order of magnitude larger than that of the athermal analog shown in part A of Figure 9. The *average* copolymer stiffness controls both the overall melt compressiblity and the precise magnitude of $\Delta g(r)$ at low temperatures. Just as the thermally-induced changes in the *individual* radial distribution functions are suppressed for stiffer chains, the magnitude of $\Delta g(r)$ decreases with increasing overall copolymer stiffness (or fluid density (not shown)) *at a fixed distance from the apparent spinodal.*

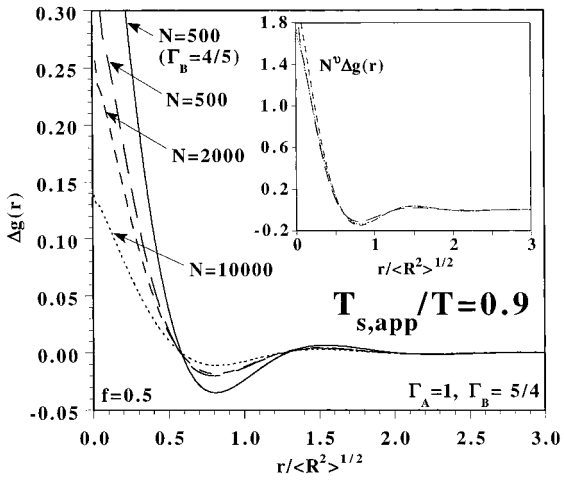

Figure 10. Influence of chain asymmetries and chain length on low temperature clustering. Shown are the low-temperature difference functions $\Delta g(r)$ for $N = 500$, $f = 0.5$, and two different asymmetries: $\Gamma_s = {}^5/_4$, $\Gamma_f = 1$ and $\Gamma_s = 1$, $\Gamma_f = {}^4/_5$. Also shown are the cases for 2000 and 10000. The inset depicts the approximate scaling which is predicted for this clustering effect.

Figure 10 also shows the prediction for the chain length dependence of $\Delta g(r)$ at fixed (close) proximity to the apparent spinodal temperature. For structurally and interaction symmetric copolymers, the thermally driven structural modifications have a finite size in nature.[20] Within the present more realistic model this seems to hold as well since the physical mechanism for the fluctuation stabilization in PRISM theory is again a local, enthalpy-driven clustering of like monomers which couples to a microdomain length scale structure in a finite size manner via chain connectivity. However, the approach to the $N \rightarrow \infty$ asymptotic regime, where we might expect a power law decay of the fluctuation amplitude, is *very slow* and effectively irrelevant for laboratory materials. Although an *approximate* "collapse" onto a master curve as shown in the inset of Figure 10 is found, a clean scaling exponent is difficult to extract. Here $\nu \approx 0.275$, when we use the contact values (i.e. $\Delta g(r = d)$) in the fitting procedure. However, this does not reflect the asymptotic result, which appears to be somewhat *lower*. For the idealized structurally symmetric Gaussian thread model, an exponent of $\nu = {}^1/_3$ is predicted at $T_{s,app}$[28] based on the R-MPY closure, in accord with the BLFH field theory[11,12] prediction. Interestingly, the degree of collapse in the inset of Figure 10 is fairly uniform for all length scales. This suggests a coupling of fluid structure on *all* length scales and hence a common decay law of the low-temperature concentration fluctuations for the local, macromolecular, and microdomain scales. Whether this is a "crossover" effect or is indicative of the asymptotic $N \rightarrow \infty$ behavior of PRISM theory is unclear based on the present numerical results.

B. Length Scale Dependent Effective Compositions. Another way to characterize the changes that occur in fluid structure is through an effective intermolecular composition, $\Phi_{MM'}(R)$, defined by[28]

$$\Phi_{MM'}(R) = \frac{\int_0^R dr 4\pi r^2 \rho_{M'} g_{MM'}(r)}{\sum_{M''} \int_0^R dr\ 4\pi r^2 \rho_{M''} g_{MM''}(r)} \qquad (6.2)$$

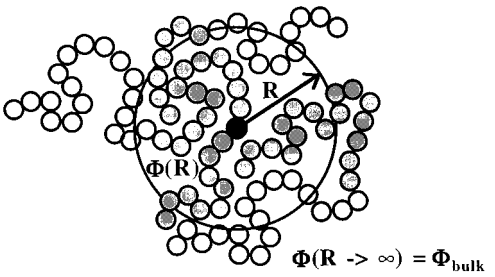

Figure 11. Illustration of the concept of length-scale-dependent "effective compositions".

This function is a measure of the *inter*molecular contribution to compositional fluctuations within a sphere of radius R about a given site.[56] Alternatively, it can be thought of as the fraction of monomers of type M' on *different* chains in a spherical volume of radius R surrounding a monomer of type M on a tagged chain. A schematic illustration of this is given in Figure 11. In the thermodynamic limit of $R \rightarrow \infty$, or the random mixing limit of $g_{MM'}(r) \approx g(r)$ for all M and M', the effective composition becomes the bulk volume fraction of species M (i.e. $\Phi_{MM} = f_M$, for the case of equal site volumes on the two blocks).

One motivation for defining such a two-point quantity comes from dynamical measurements which probe *inter*chain interactions and friction. In recent years effective local compositions have been discussed in the interpretation of dynamical measurements on copolymer and blend systems. Although a direct measurement of this quantity is not possible with present techniques, model-dependent attempts to extract such information have been made by several groups.[57−61] Depending on which experimental probe is used, the relevant value of R (i.e. the so-called "correlation radius") might be close in magnitude to the monomer size or the block size for nuclear magnetic resonance (NMR) and dielectric spectroscopy (DES) probes, respectively. SANS or SAXS experiments probe the microdomain length scale $D = 2\pi/k^*$. Recent SANS experiments[5] have perhaps found indirect evidence for sub-R_g scale clustering near the ODT. Just as the $k \approx k^*$ scattering intensity can be interpreted as a measure of concentration fluctuations on the microdomain length scale, wider angle scattering (e.g. $k \approx 2\pi/d$, where d is an *intrinsic* chemical length scale) would reveal information on these local composition fluctuations discussed here. Although we have reported our predictions in real space to provide a more concrete physical picture, these can easily be transformed into spherically averaged, wide-angle scattering patterns. Thus, with the use of a particular single chain model, the PRISM theory provides a method for interpreting such wide-angle scattering patterns in terms of effective local compositions.

Part A of Figure 12 shows the temperature dependence of the effective compositions for correlation radii of $R = 4d$ and $R = 12d$ for $f = 0.5$. As expected on the basis of the strong local enhancement of $s - s$ and $f - f$ contacts at low temperatures, the effective composition within the first few solvation shells is predicted to be the most strongly enhanced at these relatively low temperatures. The magnitudes of $\Phi_{MM}(R)$ indicate that as the fluid is cooled the immediate environment surrounding a monomer becomes pure-component-like. This may have important consequences for the observed monomeric dynamics of diblock copolymers in the melt state, as monomer friction coefficients will be sensitive to their local environments. Just as with the radial distribution functions, the values of the backbone aspect ratios change the precise magnitudes of the effective compositions with the more flexible component being more strongly perturbed at low temperature. Note also from part A of Figure 12 that there are very small athermal nonrandom-mixing contributions (corresponding to $T_{s,app}/T = 0$, not shown here) which get "washed out" by the strong clustering at low temperatures.[28] It is clear that at high temperatures both species experience similar environments characterized by an average composition.

Also shown in part A of Figure 12 is a case where we have modeled a 50% solution in a nonselective solvent by reducing the monomer number density by a factor of $^1/_2$ from the melt value. Dilution of the diblock melt with nonselective solvent increases the osmotic compressibility (or free volume) associated with the copolymer. This serves to enhance physical clustering on all length scales relative to the high concentration state and widen the nonlinear fluctuation stabilization regime as observed in $\hat{S}^{-1}(k^*)$ vs $1/T$ curves.[20] Solvent dilution also results in strong corrections to the mean field "dilution approximation" $T_s \propto \rho_{polymer}$.[49]

Part B of Figure 12 shows several different correlation radii for $\Phi_{ff}(R)$ at melt and 50% solution densities. We note that our predictions at lower densities should only be viewed as qualitative indicators of the effect relative to that in the melt, as we have not included possible chain-swelling effects or the molecularity of the solvent. Furthermore, at very low temperatures, our predictions may lead to $\Phi_{MM}(R) > 1$ which is unphysical. While the physical origin of the prediction that $\Phi_{MM}(R)$ increases as temperature is lowered is reasonable (i.e. the local clustering of like species), our somewhat arbitrary measure of proximity to a phase boundary can result in an unphysical quantitative value for $\Phi_{MM}(R)$. Curiously, it does turn out that $\Phi_{MM}(R \approx 2 - 4d) \approx 1$ at the same temperature that the scattering curve would indicate an apparent spinodal.

Part C of Figure 12 shows an example of the effective compositions for the minority and majority components in a compositionally asymmetric diblock copolymer melt where $f = 0.1$. The minority component (flexible block) pair correlation functions are strongly perturbed while the majority block is nearly unaffected even at low temperatures. Consistent with prior predictions for the structurally symmetric model,[20] the more realistic case presented here shows similar behavior. The physical picture of the arrangement of "tail" portions in the low-temperature fluctuating melt is one in which the effective composition in the region about the tagged monomer is pure-component-like, despite the fact that these monomers are dilute in the bulk sense. This is suggestive of a disordered, but highly segregated, micellar or spherical type morphology. Moreover, due to the formation of microdomains on a larger length scale, the correlations of monomers within such a region may mimic the behavior of a confined fluid (perhaps in this case a spherical pore). Calculations for strongly compositionally asymmetric diblocks of modest chain length ($N \approx 500$) in nonselective solvents ($\phi_{polymer} \approx 30\%$) show very dramatic clustering of the minority species even very far from the apparent spinodal.[62] Such strong physical clustering in nonselective solvents far from the ODT has been recently observed via microscopy by Liu et al.[63] for polystyrene−polyisosprene diblocks.

As discussed above, many of the features which develop in the low-temperature fluid near the apparent

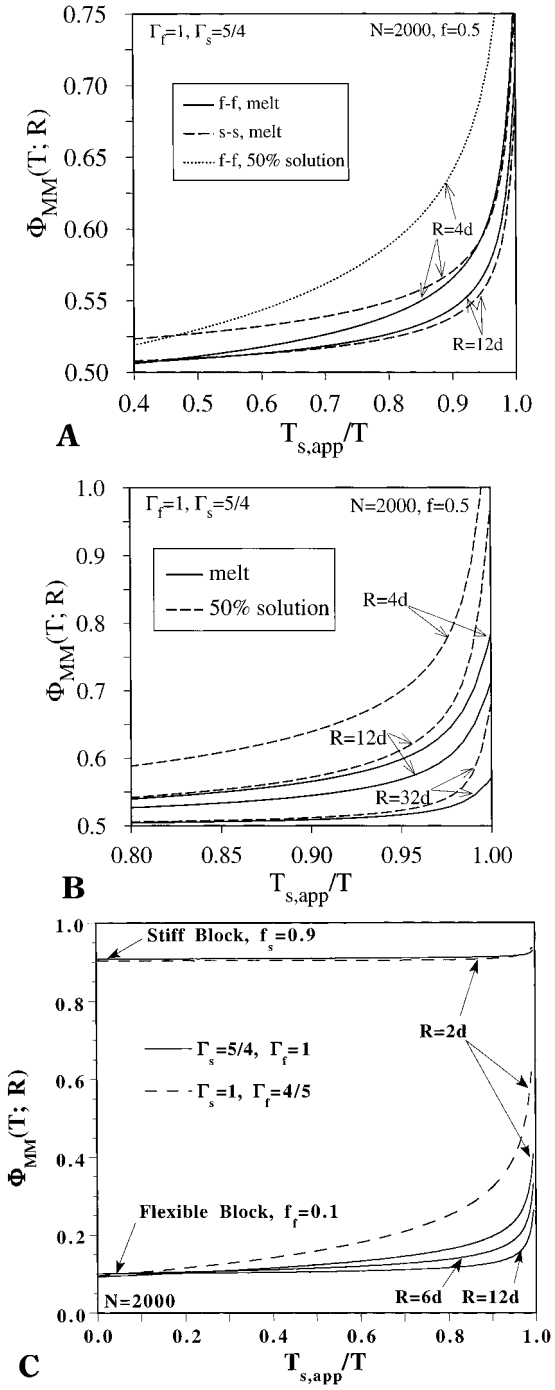

Figure 12. (A) Dependence of effective composition on correlation radius R and temperature. Shown are the cases for the flexible block (solid) and stiff block (long dash) for an $N = 2000$, $f = 0.5$, $\Gamma_f = 1$, and $\Gamma_s = {}^5/_4$ diblock copolymer. The size of the blocks are $R_{g,f} \approx 12.9d$ and $R_{g,s} \approx 16.06d$. The overall size of the diblock is $R_{g,tot} \approx 20.9d$, and the "microdomain" length scale is $D \equiv 2\pi/k^* \approx 66.1d$. Note that for $T_{s,app}/T < 0.4$ (not shown) the effective compositions are relatively temperature independent and are roughly determined by the athermal nonrandom packing correlations. The short dash is a case where the copolymer concentration is half that of the melt. (B) Comparison of the flexible−flexible length-scale-dependent compositions for the melt concentration (solid) and the 50% solution (long dash). The diblock stiffness asymmetries, composition, and chain length are the same as in part A. (C) Effective compositions for majority and minority components as a function of temperature for $N = 2000$, $f_f = 0.1$ and $f_s = 0.9$ for two different combinations of stiffness mismatch. The relevant length scales for the $\Gamma_s = {}^5/_4$, $\Gamma_f = 1$ case (solid) are $R_{g,f} \approx 5.7d$, $R_{g,s} \approx 21.6d$, $R_{g,tot} \approx 22.3d$, and $D \equiv 2\pi/k^* \approx 55.2d$. For the $\Gamma_s = 1$, $\Gamma_f = {}^4/_5$ case, $R_{g,f} \approx 4.6d$, $R_{g,s} \approx 17.3d$, $R_{g,tot} \approx 17.9d$, and $D \equiv 2\pi/k^* \approx 44.3d$.

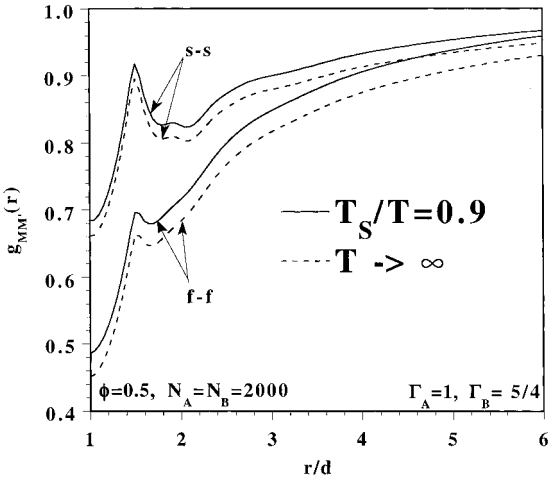

Figure 13. Radial distribution functions for a blend characterized by $N_A = N_B = 2000$, $f = 0.5$, $\Gamma_f = 1$, and $\Gamma_s = {}^5/_4$. Both the athermal limit and a thermodynamic state point close to the spinodal temperature are shown for both components. In contrast to the block copolymer, structural changes are much less pronounced.

spinodal are fairly insensitive to the details of the chain model and/or level of structural asymmetry within the range studied. For example, local compositions or the level of nonrandom mixing are most strongly influenced by the relative distance from the apparent spinodal, N, and copolymer composition, as in the simple structurally symmetric diblock.[20] Since the chain models considered above cover the range of parameters appropriate for the saturated hydrocarbons, polydienes, and other flexible diblocks, we expect similar behavior in the models of experimental systems which we considered in section V.

VII. Blend vs Diblock Behavior

Here we briefly study the differences between the above predictions for diblock copolymer melts and their binary blend counterparts. Although the quantitative degree to which their behaviors differ depends on the quantity of interest and the nonuniversal chemical and structural asymmetries, here we use the $\Gamma_s = {}^5/_4$, $\Gamma_f = 1$, $\lambda = 1$, and $\phi = 0.5$ binary blend as an example. The *apparent* spinodal was used as an approximate indicator of the microphase instability for the diblock case. On the other hand, there exists a true spinodal instability and critical point in the blend case. The ratio of the diblock T_{ODT} (or $T_{s,app}$) to the blend T_s and any deviation from its mean-field value may be an indicator of architecture dependence of the effective χ -parameter and is presently under study.

Figure 13 shows the radial distribution functions for a $N = 2000$ blend in the athermal $T \rightarrow \infty$ limit and at $T_s/T = 0.9$ (the cases studied for the diblock architecture in the previous section). As opposed to the rather large changes in the local correlations in the diblock liquid (see Figure 9), the low-temperature blend structure is well described by the athermal limit. This can be attributed to the fact that the temperature at which phase separation is predicted to be considerably higher than the corresponding apparent spinodal of the diblock. Indeed, at a fixed temperature corresponding to $T_{s,blend}$, the diblock pair correlations are also only weakly perturbed from their athermal values. This conclusion can be indirectly inferred from the effective compositions shown in part A of Figure 12. Much larger N values are needed for the diblock melt to yield such small

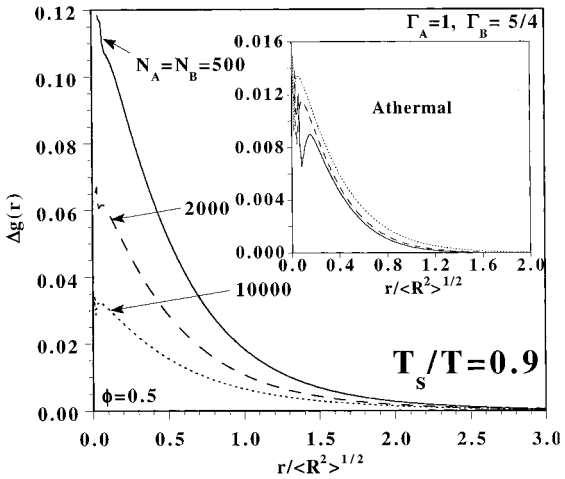

Figure 14. Difference function $\Delta g(r)$ for the blend system described in Figure 13. The inset shows the analogous $\Delta g(r)$ curves in the athermal limit.

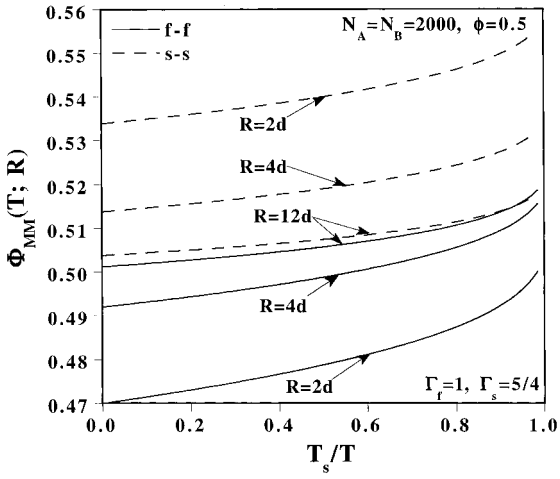

Figure 15. Temperature dependence of the length scale dependent effective compositions for the blend with $N_A = N_B = 2000$, $f = 0.5$, $\Gamma_f = 1$, and $\Gamma_s = 5/4$.

enthalpy-induced packing modifications as the corresponding blend. The fact that the blend structural correlations are well described at all relevant temperatures by the athermal "reference" system suggests that "thermodynamic perturbative" methods for calculating thermodynamic quantities are well justified. This simplification has been exploited in recent blend PRISM studies of several workers.[27,31,32]

The decay of the blend intermolecular structural fluctuations as a function of N at fixed distance from the spinodal is shown in Figure 14. Similar to the trend seen in Figure 10, $\Delta g(r)$ is smallest for large N, and the overall magnitude of the effect with respect to the diblock is small. In the athermal limit (shown in the inset of Figure 14) $\Delta g(r)$ is only weakly N-dependent, with the larger effect being for *larger* N.[29] Given these effects which act in opposite directions, the difference between $\Delta g(r)$ in the athermal and thermal case for large N is quite small. The N -scaling of the contact value is given by $\Delta g(r = d) \propto N^{-\nu}$ with $\nu \approx 0.44$, as opposed to $\nu \approx 0.275$ for the diblock case. Although these may not be asymptotic, universal scaling exponents, they clearly indicate a slower decay for the copolymer, which is expected on the basis that the diblock wave vector of maximum instability is $k^* \propto 1/R_g$ as opposed to $k = 0$ for the blend. The numerical results are similar to the large N analytic scaling behavior of $\Delta g(r = d)$ for the structurally symmetric thread model where PRISM theory, as well as field theoretic predictions, yield $\Delta g(d) \propto N^{-\nu}$, with $\nu = 1/2$ (at the spinodal temperature) for blends,[54,64] and $\nu = 1/3$ (at the ODT or extrapolated spinodal temperature) for diblock copolymers.[11,20]

Plotted in Figure 15 are both the stiff−stiff and flexible−flexible effective compositions for the blends at three length scales. Recall that for structurally asymmetric mixtures, non-random mixing in the athermal limit[29] leads to deviations in the effective compositions as well. In contrast to the copolymer case, the thermally-driven changes in $\Phi_{MM}(R)$ are small and of the same magnitude as those in the purely repulsive force fluid.

VIII. Summary and Conclusions

We have investigated the small-angle scattering profiles, apparent spinodal phase behavior, intermolecular correlations, and physical clustering in structurally asymmetric semiflexible diblock melts with attractive van der Waals interactions. A rich dependence of these quantities on conformational asymmetry was found, particularly for the apparent microphase spinodal boundaries. Contrary to the naive mean field idea that attractive forces "cancel" when the bare interactions are identical, we find that differences in the local intermolecular packing between species can result in large *effective* repulsive interactions. This coupling of the local packing correlations and enthalpic interactions leads to phase behavior which depends on the degree of structural asymmetry in the diblock molecule.

The finite hard core diameter calculations were also compared to the idealized analytical thread model predictions,[21] and general consistency was found at least for large N. This suggests the simple thread model serves as a reliable indicator of the behavior of more realistic models within the framework of PRISM theory. We also compared the predicted trends in polyolefin diblock melts with experimental data of Bates et al.[1,5] Even for the extreme $\chi_o \equiv 0$ case, the structural disparities result in strong dependencies of the apparent microphase spinodal boundaries on stiffness asymmetry consistent with experiment. However, we caution that the use of unbranched effective semiflexible chain models may not always yield quantitative predictions. Further studies with atomistic chain models are required to shed light on this important question.

The local intermolecular structure was also studied. Most of the *very* local structural features present in the athermal melt are retained as temperature is decreased. However, this short wavelength "fine structure" is superimposed on an overall enhancement (g_{AA}, g_{BB}) or depletion (g_{AB}) of contacts as the apparent spinodal is approached. This strong local clustering is accompanied by the buildup of a longer wavelength oscillatory feature in the pair correlations which reflects the formation of A-rich and B-rich microdomains. Although athermal entropic packing considerations lead to the stiffer component having a larger $g(r)$ near contact, this trend can sometimes be reversed at low temperatures as a result of the more flexible component being less stable to long wavelength concentration fluctuations, as indicated by the species dependent collective structure factors $S_{MM'}(k \approx k^*)$. Dilution of the melt by nonselective solvent can enhance physical clustering very significantly due to the increased copolymer osmotic compressiblity. For highly asymmetric copolymer compositions, we find that the majority component pack-

ing remains nearly unperturbed as the fluid segregates. On the other hand, the minority block experiences a marked change from its athermal environment. In this case, the effective composition within shells of order the monomer size are strongly enhanced and approach the pure component limit near the apparent spinodal. To zeroth order, most of the thermally-induced structural changes appearing in the calculations presented here are very similar to those found in the idealized symmetric model with a repulsive AB tail potential.[20]

Finally, both the Gaussian thread and finite hard core diameter models indicate a high sensitivity of the spinodal phase boundaries on conformational mismatch. Thus, accounting for chain stretching effects at low temperatures,[41] however small, may impact the absolute temperature scale as well as the nature of the asymmetry in T_{ODT} vs f phase diagrams. That is, the possiblity that $\gamma = \gamma(T,f) \neq \Gamma_{B,pure}/\Gamma_{A,pure}$, due to nonideal conformational effects, as well as the differences between an extrapolated spinodal temperature and the real first order microphase separation temperature, potentially complicates the comparison of our results with experimental ODT phase boundaries. However, our previous theoretical work,[41] the results of several simulations,[65] and recent experiments,[66] all suggest that relatively small conformational changes occur near the ODT. Finally, we believe our *general* conclusions regarding the liquid structure are largely insensitive to the precise conformational properties, suggesting a common, enthalpy-driven fluctuation stabilization phenomenon occurs at low temperatures for all flexible diblock systems.

Acknowledgment. This work was supported by the U.S. Department of Energy via Sandia National Laboratories CRADA #1087. Use of the central computing facilities of the Materials Research Laboratory at UIUC (DEFG02-91ER45439) is gratefully acknowledged.

References and Notes

(1) Bates, F. S.; Schultz, M. F.; Rosedale, J. H. *Macromolecules* **1992**, *25*, 5547.
(2) Walsh, D. J.; Graessley, W. W.; Datta, S.; Lohse, D. J; Fetters, L. J. *Macromolecules* **1992**, *25*, 5236. Graessley, W. W.; Krishnamoorti, R.; Balsara, N. P.; Fetters, L. J.; Lohse, D. J.; Schultz, D. N.; Sissano, J. A. *Macromolecules* **1994**, *27*, 2574. Graessley, W. W; Krishnamoorti, R.; Balsara, N. P.; Butera, R. J.; Fetters, L. J.; Lohse, D. J.; Schultz, D. N.; Sissano, J. A. *Macromolecules* **1994**, *27*, 3896. Krishnamoorti, R.; Graessley, W. W.; Dee, G. T.; Walsh, D. J.; Fetters, L. J.; Lohse, D. J. *Macromolecules* **1996**, *29*, 367.
(3) Rhee, J.; Crist, B. *Macromolecules* **1991**, *24*, 5663. Graessley, W. W.; Krishnamoorti, R.; Balsara, N. P.; Fetters, L. J.; Lohse, D. J.; Schultz, D. N.; Sissano, J. A. *Macromolecules* **1994**, *27*, 3073. Crist, B.; Hill, M. J. *J. Polym. Sci., Polym. Phys.* in press.
(4) Gehlsen, M. D.; Bates, F. S. *Macromolecules* **1994**, *27*, 3611.
(5) Rosedale, J. H.; Bates, F. S.; Almdal, K.; Mortensen, K.; Wignall, G. D. *Macromolecules* **1995**, *28*, 1429.
(6) Bates, F. S.; Fredrickson, G. H. *Annu. Rev. Phys. Chem.* **1990**, *41*, 525.
(7) Bates, F. S. *Science* **1991**, *251*, 898.
(8) Leibler, L. *Macromolecules* **1980**, *13*, 1602.
(9) Helfand, E. *J. Chem. Phys.* **1975**, *62*, 999.
(10) For a review, see: Matsen, E.; Bates, F. S. *Macromolecules* **1996**, *29*, 2092.
(11) Fredrickson, G. H.; Helfand, E. *J. Chem. Phys.* **1987**, *87*, 697.
(12) Brazovskii, S. A. *Sov. Phys. JETP (Engl. Transl.)* **1975**, *41*, 85.
(13) Barrat, J.; Fredrickson, G. H. *J. Chem. Phys.* **1991**, *95*, 1281.
(14) Vilgis, T. A.; Borsali, R. *Macromolecules* **1990**, *23*, 3172.
(15) Olvera de la Cruz, M. *Phys. Rev. Lett.* **1991**, *67*, 85. Mayes, A. M.; Olvera de la Cruz, M. *Macromolecules* **1991**, *24*, 3975. Mayes, A. M.; Olvera de la Cruz, M. *J. Chem. Phys.* **1991**, *95*, 4670.
(16) Stepanow, S. *Macromolecules* **1995**, *28*, 8233.
(17) Melenkevitz, J.; Muthukumar, M. *Macromolecules* **1991**, *24*, 4199.
(18) Lescanec, R. L.; Muthukumar, M. *Macromolecules* **1993**, *26*, 3908.
(19) Freed, K. F.; Dudowicz, J. *J. Chem. Phys.* **1992**, *97*, 2105. Dudowicz, J.; Freed, K. F. *Macromolecules* **1993**, *26*, 213. Dudowicz, J.; Freed, K. F. *J. Chem. Phys.* **1993**, *99*, 4804. Dudowicz, J.; Freed, K. F. *J. Chem. Phys.* **1994**, *100*, 4653.
(20) David, E. F.; Schweizer, K. S. *J. Chem. Phys.* **1994**, *100*, 7767, 7784.
(21) Schweizer, K. S. *Macromolecules* **1993**, *26*, 6033, 6050.
(22) Hołyst, R.; Schick, M. *J. Chem. Phys.* **1991**, *96*, 730.
(23) Liu, A. J.; Fredrickson, G. H. *Macromolecules* **1992**, *25*, 5551.
(24) Singh, C.; Goulian, M.; Liu, A. J.; Fredrickson, G. H. *Macromolecules* **1994**, *27*, 2974.
(25) Fredrickson, G. H.; Liu, A. J.; Bates, F. S. *Macromolecules* **1994**, *27*, 2503. Bates, F. S.; Fredrickson, G. H. *Macromolecules* **1994**, *27*, 1065. Fredrickson, G. H.; Liu, A. J. *J. Polym. Sci., Polym. Phys.* **1995**, *33*, 1203.
(26) Matsen, M. W.; Schick, M. *Macromolecules* **1994**, *27*, 4014.
(27) Schweizer, K. S.; Singh, C. *Macromolecules* **1995**, *28*, 2063.
(28) David, E. F.; Schweizer, K. S. *Macromolecules* **1995**, *28*, 3980.
(29) Singh, C.; Schweizer, K. S. *J. Chem. Phys.* **1995**, *103*, 5814.
(30) Dudowicz, J.; Freed, K. F. *Macromolecules* **1996**, *29*, 625.
(31) Rajasekaran, J. J.; Curro, J. G.; Honeycutt, J. D. *Macromolecules* **1995**, *28*, 6843.
(32) Singh, C.; Schweizer, K. S. *Macromolecules* **1995**, *28*, 8692. Singh, C.; Schweizer, K. S. *Macromolecules* **1997**, *30*, 1490.
(33) Weinhold, J.; Kumar, S.; Singh, C.; Schweizer, K. S. *J. Chem. Phys.* **1995**, *103*, 9460. Kumar, S.; Weinhold, J. *Phys. Rev. Lett.* **1996**, *77*, 1512.
(34) Grest, G. S. Private communication.
(35) Micka, U.; Binder, K. *Macromol. Theory Simul.* **1995**, *4*, 419.
(36) Chandler, D. In *Studies in Statistical Mechanics VIII*; Montroll, E. W., Lebowitz, J. L., Eds.; North-Holland: Amsterdam, 1982; pp 275−340.
(37) Schweizer, K. S.; Curro, J. G. *Phys. Rev. Lett.* **1987**, *58*, 246. Curro, J. G.; Schweizer, K. S. *J. Chem. Phys.* **1987**, *87*, 1842. Schweizer, K. S.; Curro, J. G. *Macromolecules* **1988**, *21*, 3070.
(38) For reviews, see: Schweizer, K. S.; Curro, J. G. *Adv. Polym. Sci.* **1994**, *116*, 319. Schweizer, K. S.; Curro, J. G. *Adv. Chem. Phys.* **1997**, *vol. 98* p 1.
(39) This need not be done. For treatments of the inter- and intramolecular self-consistency problem in the homopolymer context, see ref 40. See ref 41 for the case of diblock copolymers.
(40) Schweizer, K. S.; Honnell, K. G.; Curro, J. G. *J. Chem. Phys.* **1992**, *96*, 3211. Melenkevitz, J.; Curro, J. G.; Schweizer, K. S. *J. Chem. Phys.* **1993**, *99*, 5571. Melenkevitz, J.; Schweizer, K. S.; Curro, J. G. *Macromolecules* **1993**, *26*, 6190. Grayce, C. J.; Schweizer, K. S. *J. Chem. Phys.* **1994**, *100*, 6846. Grayce, C. J.; Yethiraj, A.; Schweizer, K. S. *J. Chem. Phys.* **1994**, *100*, 6857.
(41) David, E. F.; Schweizer, K. S. *J. Chem. Soc., Faraday Trans.* **1995**, *91*, 2411.
(42) Yethiraj, A.; Schweizer, K. S. *J. Chem. Phys.* **1992**, *97*, 5927.
(43) Schweizer, K. S.; Yethiraj, A. *J. Chem. Phys.* **1993**, *98*, 9053. Yethiraj, A.; Schweizer, K. S. *J. Chem. Phys.* **1993**, *98*, 9080.
(44) Hansen, J. P.; McDonald, I. R. *Theory of Simple Liquids*; Academic Press: London, 1986.
(45) Schweizer, K. S.; David, E. F.; Singh, C.; Curro, J. G.; Rajasekaran, J. J. *Macromolecules* **1995**, *28*, 1528.
(46) Curro, J. G. *Macromolecules* **1994**, *27*, 4665.
(47) Honnell, K. G.; Curro, J. G.; Schweizer, K. S. *Macromolecules* **1990**, *23*, 3496.
(48) Experiments generally find that the actual ODT temperature is lower than the extrapolated spinodal value. See, for example, ref 5.
(49) Guenza, M.; Schweizer, K. S. *J. Chem. Phys.* **1997**, *106*, 7391. Guenza, M.; Schweizer, K. S. *Macromolecules* **1997**, *30*, 4205.
(50) Curro, J. G.; Schweizer, K. S. *Macromolecules* **1990**, *23*, 1402.
(51) We note that even within the analytical thread model, the (linearized) R-MPY theory predicts a destruction of $k \neq 0$ spinodal instabilities. This expression is the asymmetric copolymer analog to the HTA or extrapolated part of the full fluctuation expression discussed in ref 20.
(52) Here, we use the notation of N_{seg} as defined in ref 1. For the PE case, one segment has $4CH_2$ units and hence $N = 4\ N_{seg}$ if we take each site to correspond to a CH_2 as done in this work.
(53) McCoy, J. D.; Mateas, S.; Zorlu, M.; Curro, J. G. *J. Chem. Phys.* **1995**, *102*, 8635. Han, J.; Boyd, R. H. *Macromolecules*

1994, *27*, 5365. Toxvaerd, S. *J. Chem. Phys.* **1990**, *93*, 4290. Paul, W.; Yoon, D. Y.; Smith, G. D. *J. Chem. Phys.* **1995**, *103*, 1702.

(54) Singh, C.; Schweizer, K. S.; Yethiraj, A. *J. Chem. Phys.* **1995**, *102*, 2187.

(55) For AB copolymers, there are three distinct structure factors: $\hat{S}_{AA}(k)$, $\hat{S}_{BB}(k)$, and $\hat{S}_{AB}(k)$. We define an average reciprocal structure factor as $\langle \hat{S}^{-1}(k) \rangle = [1/\hat{S}_{AA}(k) + 1/\hat{S}_{BB}(k) - 2/\hat{S}_{AB}(k)]/4$.

(56) It is important to note that these effective composition variables differ from the *one-body* composition fields usually discussed in the context of block copolymer field theories. The quantities of eq 6.2 are related to *two*-point *inter*molecular distribution functions and describe the composition associated with different chains in a given region of space about a reference site on a tagged chain.

(57) Quan, X.; Johnson, G. E.; Anderson, E. W.; Bates, F. S. *Macromolecules* **1989**, *22*, 2451.

(58) Alig, I.; Kremer, F.; Fytas, G.; Roovers, J. *Macromolecules* **1992**, **25**, 5277.

(59) Stühn, B.; Stickel, F. *Macromolecules* **1992**, *25*, 5306.

(60) Fytas, G.; Anastasiadis, S. H.; Karatasos, K.; Hadjichristidis, N. *Phys. Scr.* **1993**, *T49A*, 237.

(61) Chung, G.-C.; Kornfield, J. A. *Macromolecules* **1994**, *27*, 964.

(62) Kolbet, K.; Schweizer, K. S. Unpublished work.

(63) Liu, Z.;Kobayashi, K.; Lodge, T. *J. Polym. Sci., Polym. Phys.*, submitted for publication, 1996.

(64) Hołyst, R.; Vilgis, T. A. *J. Chem. Phys.* **1993**, *99*, 4835.

(65) See, for example: Fried, H.; Binder, K. *J. Chem. Phys.* **1991**, *94*, 8349. Weyersburg, A.; Vilgis; T. A. *Phys. Rev. E.* **1993**, *48*, 377. Binder, K.; Fried H. *Macromolecules* **1993**, *26*, 6878. Hofferman, A.; Sommer, J.-U.; Blumen, A. *J. Chem. Phys.* **1997**, *106*, 6709.

(66) Bartels, V. T.; Stamm, M.; Abetz, V.; Mortensen, K. *Europhys. Lett.* **1995**, *31*, 81.

MA970202O